



Multiple sources of atmospheric CO₂ activated by AMOC recovery at the onset of interglacial MIS 9

Florian Krauss^{a,1} , Daniel Baggenstos^{b,c} , Jochen Schmitt^a , Béla Tuzson^d , James A. Menking^{c,e} , Lars Mächler^a, Lucas Silva^a , Markus Grimmer^a , Emilie Caproni^f , Thomas F. Stocker^a, Thomas K. Bauska^g , and Hubertus Fischer^a

Affiliations are included on p. 8.

Edited by Mark Thiemens, University of California San Diego, La Jolla, CA; received November 6, 2024; accepted April 23, 2025

Using high-precision ice core measurements of CO₂, δ¹³C–CO₂, CH₄, and N₂O, this study provides carbon isotope constraints on a sizeable, centennial-scale CO₂ jump at the onset of Marine Isotope Stage 9 (MIS 9). The very end of the Heinrich stadial (HS) characterizing Termination IV (T-IV, ca. 343 to 333 ka ago) shows a 250-y-long jump in greenhouse gas concentrations, followed by a 1.3 ka gradual decline back to the initial concentration. During this so-called overshoot, CO₂ and CH₄ reach their highest levels (about 303 ppm and 800 ppb, respectively) over the past 800 ka prior to industrialization. The jump in CO₂ is not accompanied by a change in δ¹³C–CO₂, suggesting that multiple mechanisms contributed to the exceptionally elevated CO₂ values. Following the jump, a slow 0.2‰ enrichment in δ¹³C–CO₂ occurs. We propose that during the jump, the sudden resumption of deepwater formation in the North Atlantic (NA) triggered an amplified release of CO₂ from the Southern Ocean (SO) by a northward shift of the Intertropical Convergence Zone (ITCZ) and the SO westerlies, potentially in combination with a rapid land carbon release. The latter is expected from temporally enhanced wildfire activity related to higher fuel load and regionally changing weather conditions in connection to the ITCZ shift. A combination of marine proxy records and box model simulation suggests that the δ¹³C–CO₂ decrease expected from these processes is compensated by a net temperature increase in global sea surface temperature (SST) at the time of the AMOC resumption.

ice cores | paleoclimate | carbon cycle | stable carbon isotopic composition | Termination IV

Atmospheric CO₂ plays a key role in the recent but also past climate evolution, and the CO₂-climate feedback is crucial to quantitatively explain the glacial/interglacial temperature amplitude. Ice core records over the last 800 ka reveal a high correlation of CO₂ and Antarctic temperature on glacial/interglacial (1–3) and millennial time scales (1, 4).

The millennial-scale CO₂ variations are an expression of the thermal bipolar seesaw (5), imprinting a two-phased pattern on Antarctic and North Atlantic (NA) temperature recorded in paleoclimate archives. The “stadial” phase is characterized by a reduced Atlantic Meridional Overturning Circulation (AMOC; 6, 7), cool NA temperature, and a gradual increase of Antarctic temperature and atmospheric CO₂. These millennial CO₂ increases, on the order of 20 ppm, are most pronounced during extended Heinrich stadials (HS), when the AMOC was significantly reduced (6, 7) and Antarctic temperature reconstructions based on ice cores show a slow increase by about 3 °C (8). The “interstadial” phase, triggered by AMOC resumption, is marked by an abrupt warming event in the NA (Dansgaard-Oeschger (DO) event), and ensuing Antarctic cooling and decreasing CO₂.

This bipolar connectivity through ocean circulation and heat storage has been clearly documented in data (9) and models (10, 11). However, the concurrent carbon cycle response is not well understood. On millennial time scales, the observed CO₂ variations likely reflect varying storage of respired carbon in the deep ocean. Such a role of ocean carbon storage is corroborated by δ¹³C–

CO₂ evidence from Antarctic ice cores, suggesting the removal of isotopically depleted carbon from the atmosphere during the descent into stadial conditions (12, 13) and its release after the onset of HS warming in the Southern Ocean (SO; 14, 15). While climate models are able to simulate the thermal bipolar seesaw response, coupled carbon climate models produce varying results concerning the atmospheric CO₂ response to AMOC changes (16). The cause of millennial CO₂ variations, thus, cannot be unambiguously attributed by models yet. Changes in ocean ventilation, iron fertilization in the SO, sea surface temperature (SST), and changes in land carbon storage related to DO events are all contributing mechanisms.

Significance

Prior to the Industrial Period, the highest levels of CO₂ and CH₄ over the last 800 ka occurred about 335 ka ago, at which time both gases rapidly increased before tailing back down over the next 1.3 ka. Here, we characterize these changes using new data for all three greenhouse gases (CO₂, CH₄, and N₂O) and, most crucially, the first measurements of the stable carbon isotopes of CO₂. We propose that this jump is caused by an enhanced release of CO₂ from the Southern Ocean likely in combination with a release of land carbon through wildfires as the result of an abrupt resumption of deep ocean circulation in the Atlantic, leading to changes in global atmospheric circulation and precipitation.

Author contributions: F.K., D.B., J.S., and H.F. designed research; F.K., L.S., M.G., E.C., T.F.S., and T.K.B. performed research; F.K., B.T., and L.M. contributed new reagents/analytic tools; F.K. analyzed data; and F.K., J.M., and H.F. wrote the paper.

The authors declare no competing interest.

This article is a PNAS Direct Submission.

Copyright © 2025 the Author(s). Published by PNAS. This article is distributed under [Creative Commons Attribution-NonCommercial-NoDerivatives License 4.0 \(CC BY-NC-ND\)](https://creativecommons.org/licenses/by-nc-nd/4.0/).

PNAS policy is to publish maps as provided by the authors.

¹To whom correspondence may be addressed. Email: florian.krauss@unibe.ch.

This article contains supporting information online at <https://www.pnas.org/lookup/suppl/doi:10.1073/pnas.2423057122/-/DCSupplemental>.

Published June 2, 2025.

Only recently, with the advent of higher precision and higher-resolution Antarctic CO₂ records (17–19), rapid, centennial-scale carbon dioxide jumps (CDJ) on the order of 5 to 15 ppm could be identified, which have no analog in Antarctic temperature. CDJs are detected within HSs, called “CDJ–” events, and presumably occurring at the time of major Heinrich iceberg discharge events (HE) in the NA, during the last and previous glacials (17–19). Jumps are also found at the onset of some DO events, referred to as “CDJ+” events, during Marine Isotope Stage (MIS) 5, MIS 8, and MIS 10 (12, 18, 19). CDJ+ events are not so clearly detected within MIS 3 (17), however, CDJ+ events are also prominently observed at the time of rapid warmings during the last (20, 21) and previous glacial terminations (18, 19). The short time scale of CDJ events suggests additional processes are at play besides the adjustment of deep ocean carbon storage.

It has been shown that DO events not only have a slow oceanic teleconnection with the SO through the bipolar seesaw but also a fast atmospheric teleconnection through shifts in the Intertropical Convergence Zone (ITCZ) and the westerly wind belts (22, 23). Accordingly, the CDJ– occurring during HEs of the last glacial period has been attributed to a southward shift of the ITCZ [also imprinted in CH₄ anomalies attributed to emissions by Southern Hemisphere (SH) wetlands (24, 25)], which is likely connected to a strengthening and potential southward shift of the SO westerlies, when AMOC is abruptly reduced. A wind-driven CO₂ release of a few ppm has also been observed for increased SO westerly wind stress in coupled climate-carbon cycle models (25–27), while models suggest reduced CO₂ outgassing for a southward shift of the westerlies without intensification (25, 28). A decline in CO₂ is observed for weakened SO westerlies but an increase in case of a northward shift of the SO westerlies in the models. New work on the isotopic signature of CH₄ (29) demonstrated a plausible intermittent release of CH₄ and CO₂ from wildfires triggered by meridional wind shifts at HE methane pulses and the onset of DO events, which could explain at least part of the up to 10 ppm increase during CDJ+.

An unambiguous quantitative explanation in terms of the accompanying carbon cycle changes is still missing for the CDJ+ events that parallel the onset of DO events and the rapid warmings observed in the Northern Hemisphere (NH) that conclude glacial/interglacial terminations over the entire ice core record, and which are all connected to a prominent synchronous rapid increase in atmospheric CH₄ (18). The most prominent of these late termination/early interglacial CDJ+ events happened at the end of T-IV (ca. 334.6 ka), when a sudden CO₂ jump of about 15 ppm in 250 y led to the highest CO₂ concentration of 303 ppm in the entire preindustrial ice core record (18). In the following 1.3 ka, the CO₂ concentration decreases to typical interglacial values of around 280 ppm (18). In this study, we describe this event in more detail by presenting high-precision CO₂, CH₄, and N₂O as well as δ¹³C–CO₂ measurements over T-IV and the following interglacial, with a special focus on the fast CO₂ response at the onset of MIS 9, hereafter called the overshoot.

The measurements in this study were performed using a sublimation extraction and dual-laser spectroscopy method (30), which allows us to simultaneously measure all these parameters on a single ice core sample (31). Besides further improving the temporal resolution of the already available records at that point in time, we, most importantly, provide the first δ¹³C–CO₂ constraint over this time interval and make use of the co-occurring changes in CH₄ and N₂O, together with marine and terrestrial records, to describe the climate context of this overshoot. In order to test carbon cycle hypotheses to explain i) this event, ii) the predating deglacial boundary conditions leading to it, and iii) its relaxing phase, we combine our high precision CO₂ and δ¹³C–CO₂ ice

core measurements with marine carbon cycle proxies and carbon cycle box model results.

Materials and Methods

A novel analytical system based on Laser Induced Sublimation Extraction coupled to Quantum Cascade Laser Absorption Spectroscopy (LISE–QCLAS) has been developed to extract and jointly quantify CO₂, CH₄, N₂O, as well as δ¹³C–CO₂ in ice core samples. Using air samples of only 1.5 mL STP extracted from the ice core samples, we simultaneously quantify the greenhouse gas concentrations with a precision (1σ) of 0.4 ppm, 3 ppb, 1 ppb, and 0.04‰ for CO₂, CH₄, N₂O, and δ¹³C–CO₂, respectively (30). Since sublimation achieves 100% extraction efficiency, a discrimination between smaller and bigger clathrates, which may differ in their gas composition (32, 33), is avoided. The method was developed to achieve a semicontinuous vertical resolution of 1 to 2 cm in highly thinned ice cores, sublimating 10 to 15 g of ice for one measurement. However, in this study, we do not exploit the high-resolution capability for continuous measurements, but rather use the sublimation extraction to obtain high-precision replicate measurements on discrete samples of 5.5 cm length each (*SI Appendix*). A detailed description of the extraction step and quantification of greenhouse gas concentration has been published elsewhere (30, 34).

Results and Discussion

Heinrich Stadial during T-IV—Setting the Scene for the CO₂ Overshoot. The principal mechanism underlying the initiation of a HS is attributed to a reduction of the AMOC, triggering the thermal bipolar seesaw via an oceanic teleconnection. This phenomenon leads to very cold conditions in the NH, in particular, the NA region, and a slow concurrent warming of the SH (5, 6, 11, 35) reflected in the Antarctic water isotope record [Fig. 1*A*; (36)]. Deglacial HS culminate in a rapid and extensive HE in the NA (37) associated with intense calving of ice bergs and ice-sheet break-up in the NH (38), which is likely also related to a minimum in deep water formation in the NA. Extended, strong HSs are typical features of ice ages and specifically of the last two glacial terminations (39) and during T-IV (Fig. 1; green box)

The initiation of the HS during T-IV (and the AMOC reduction) coincides with a multi-centennial scale CO₂ increase (CDJ-10a) of 15 ppm between 341.9 and 341.3 ka [Fig. 1*B*; (18)]. Following CDJ-10a, a more gradual 17 ppm CO₂ increase and minor concentration changes of CH₄ and N₂O between 341.3 and 339.2 ka are found, which are accompanied by a continuous 0.5‰ depletion in δ¹³C–CO₂ (–6.87 to –7.33‰; Fig. 1*C*). Although distinct in amplitude and rate of change, a similar drop of δ¹³C–CO₂ connected to an increase in CO₂ was observed after the onset of T-I (0.4‰ depletion and 28 ppm increase), T-II [0.14‰ depletion and 27 ppm increase; (15, 33, 48)] and HS 6 [0.54‰ depletion and 21 ppm increase; (12, 13)] and attributed to the release of respired carbon from the SO. For T-I, it was argued that the sea ice in the SO retreated and enhanced mixing, i.e., rapid ventilation, deepened the mixing front so that water masses previously isolated from the atmosphere upwelled north of the sea ice edge (49). As a result, carbon-rich waters were lifted to the surface, where CO₂ outgassed to the atmosphere (Fig. 2). The stable isotope studies of Bauska et al. (48) and Schmitt et al. (15) agree on a depletion of δ¹³C–CO₂ expected from the release of respired carbon from the SO at the onset of T-I. Consistent with other terminations, our data show that the strong depletion in δ¹³C–CO₂ occurs alongside the onset of warming and the rise in deuterium excess in Antarctica, as a possible indicator of greater moisture delivery [Fig. 1*F*; (40)], and a drop in dust particle concentration [Fig. 1*H*; (42)], suggesting that all three mechanisms of sea-ice retreat, rapid ventilation, and iron fertilization are likely playing a role in this crucial, early phase of the termination.

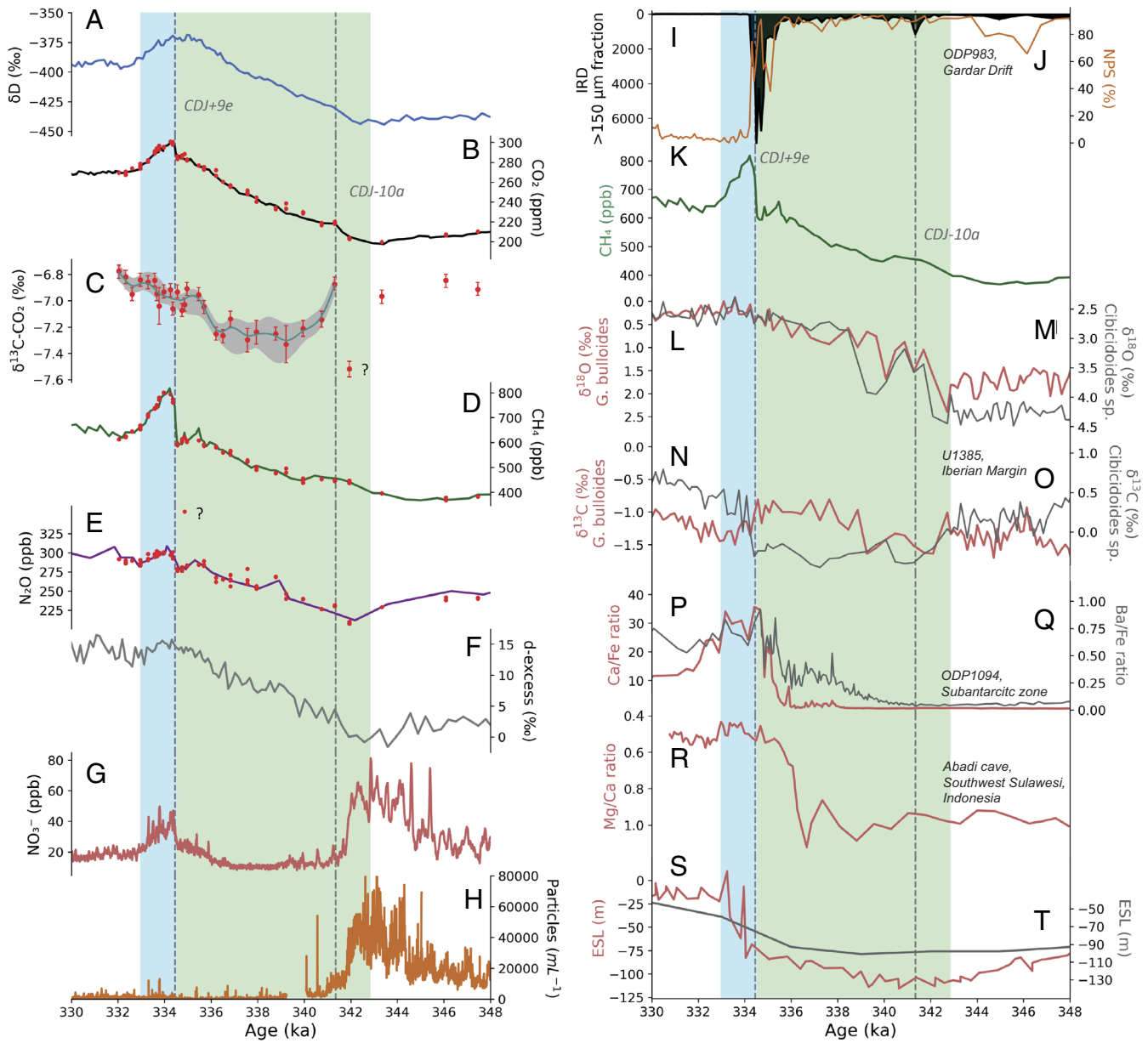


Fig. 1. EDC Ice core records (Left panel), Marine sediment and speleothem records (Right panel) during T-IV. The green box indicates the HS, the blue box the overshoot. Left panel: (A) EDC δD [blue, (36)]. (B) EDC CO_2 concentration [black line (18)], red dots this study. (C) EDC $\delta^{13}C-CO_2$ signature [cyan corresponds to a Monte Carlo spline approximation (MCA), gray band corresponds to its 1σ uncertainty, this study]. (D) EDC CH_4 concentration [green line (18)], red dots this study. (E) EDC N_2O concentration (magenta) and red dots, this study. (F) EDC deuterium excess [gray, (40)]. (G) EDC NO_3^- concentration [red, (41)]. (H) EDC dust particle concentration [orange, (42)]. Right panel: (I) and (J) IRD (black area) and NPS ratio (orange line) from ODP983, Gardar Drift, North Atlantic, (37). (K) EDC CH_4 concentration as in (D). (L and M) $\delta^{18}O$ *G. bulloides* (red) and $\delta^{18}O$ *Cibicides* sp. (gray) from U1385, Iberian Margin, (43). (N and O) $\delta^{13}C$ *G. bulloides* (red) and $\delta^{13}C$ *C. wuellerstorfi* (gray), (43). (P and Q) Ca/Fe (red) and Ba/Fe ratio (gray) from ODP1094, Atlantic sector of the Subantarctic Zone, (44). (R) Stalagmite Mg/Ca ratio (red) from Abadi cave in southwest Sulawesi, Indonesia (45). (S) ESL sea level [(46); red] and (T) ESL sea level (47); gray. All ice core records on the AICC23 age scale; all other records on their original age scales.

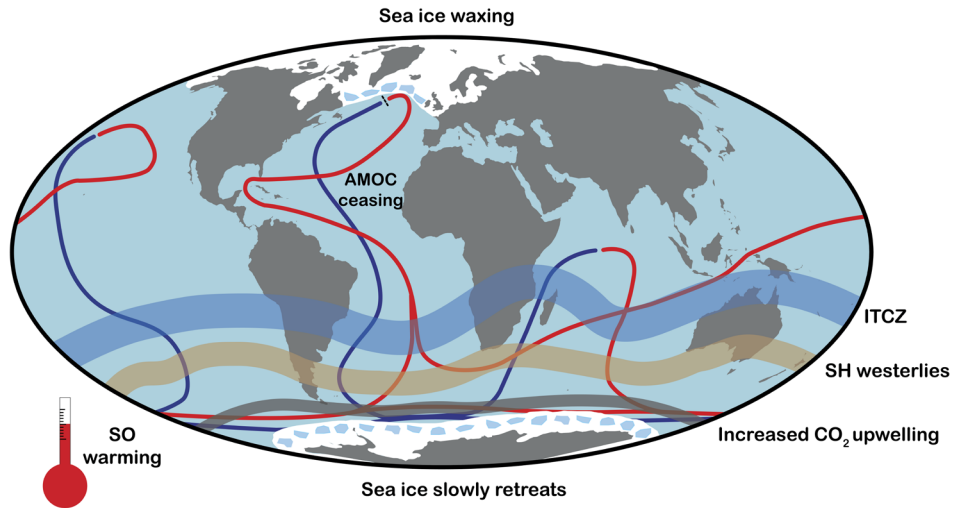
In line with a strong reduction of deep water formation in the NA during T-IV, marine records from the Iberian Margin reveal a strong decoupling of $\delta^{13}C$ in the planktic foraminifera species *G. bulloides* and $\delta^{13}C$ in the benthic foraminifera *C. wuellerstorfi* throughout the HS, pointing toward reduced deep convection in the NA [Fig. 1 N and O; (43)] and benthic foraminifera to be bathed in southern-sourced waters. In addition, the benthic $\delta^{18}O$ signal of *Cibicides* sp. resembles the stable water isotope record in Antarctic ice cores (50, 51) providing evidence of increasing temperatures in the SH carried northward by the southern-sourced water into the deep NA at the Iberian Margin (Fig. 1M).

The interval of the termination between 339.2 and 334.5 ka is characterized by slow but large increases in CO_2 and CH_4 of 34

ppm and 105 ppb, respectively. $\delta^{13}C-CO_2$ shows overall only minor changes around a level of -7.25‰ during the same interval, followed by a 0.2‰ enrichment from -7.2 to -7.0‰ at around 336 ka (Fig. 1C). The deglacial HS culminates in a final extensive ice berg calving event in the NA (37) starting at around 335 ka (Fig. 1I).

We conclude that, despite the limited proxy availability compared to T-I and T-II, our $\delta^{13}C-CO_2$ data are consistent with T-IV being characterized by a long-lasting AMOC perturbation associated with a HS and a slow release of respired carbon from the SO, largely in line with the scenario proposed for T-I (15, 48, 49) with the difference that T-IV lacks a reversal analogous to the Younger Dryas cold interval during T-I.

Heinrich Stadial



Overshoot

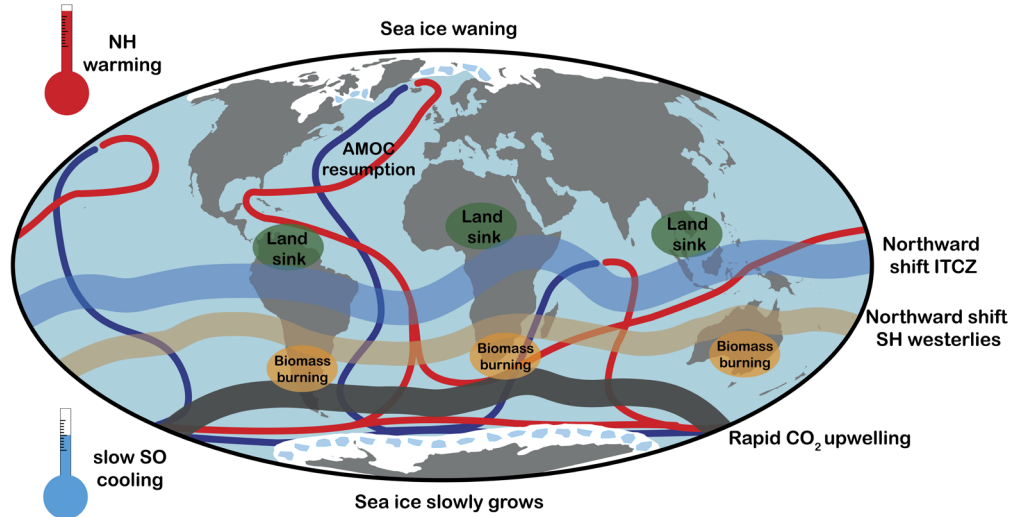


Fig. 2. A general process illustration showing the underlying mechanisms connecting sea ice coverage, AMOC strength, positioning of ITCZ and SH westerlies, as well as CO₂ sinks and sources of the Heinrich stadial (334.6 to 343 ka) and the Overshoot (334.6 to 332.9 ka) during T-IV. Upper illustration: Ceasing of the AMOC warmed the SO, leading to a southward shift of the ITCZ and SH westerlies (note that the southward location of the ITCZ in this figure is not exact but for illustrative reasons). The sea ice in the SO retreated and enhanced mixing deepened the mixing front, leading to an upwelling of carbon-rich waters. Lower illustration: Resumption of the AMOC warmed the NH, leading to a rapid northward shift of the ITCZ and SH westerlies. A slow SO cooling and sea ice increase created a transient condition in which sea ice was unable to shield the ocean from enhanced isopycnal mixing and outgassing, leading to rapid CO₂ upwelling. Large-scale wetting of land ecosystems in the monsoon region enhanced carbon sequestration by land photosynthesis, partly compensating for the joint CO₂ release in the SO and by wildfires.

CO₂ Overshoot at the Onset of MIS 9. Having “set the scene” with T-IV, we turn our attention to the strong overshoot feature at the onset of MIS 9, which culminated in an abrupt increase of 15 ppm in CO₂ at 334.6 ka, 213 ppb in CH₄, and 20 ppb in N₂O (Fig. 3 A, C, and D; further on referred to as jump) followed by a gradual (1.3 ka) CO₂ decrease with a decrease rate similar in absolute values as the increase rate before the jump (Fig. 3; blue box). The total anomaly (jump and slow decrease) has a total duration of 1.5 ka (334.6 to 332.9 ka). To discern between the carbon cycle processes most likely responsible for the overshoot, we again turn to marine paleoclimate proxies for context and model results of analogous events. About the same time of the CO₂ jump, we see the rapid disappearance of

the polar-water foraminifera *N. pachyderma* at ODP983 site in the NA [Fig. 1J; (52)], the disappearance of Ice Rafted Debris [IRD; Fig. 1I; (37)], and the retreat of southern sourced waters at depth as indicated by the concurrent anticorrelated changes in planktic and benthic δ¹³C [Fig. 1N and O; (43)]. We interpret these changes as signs of a sudden resumption of deepwater formation in the NA, connected to rapid warming (53) but also atmospheric changes in the NA region (54, 55). Earth-system model results suggest that convection in the South Labrador Sea could reach depths of 3,000 to 4,000 m during an abrupt resumption of the AMOC, following a period of weakened overturning as expected for an extended HE (56). Furthermore, an overshoot of the AMOC occurs directly at

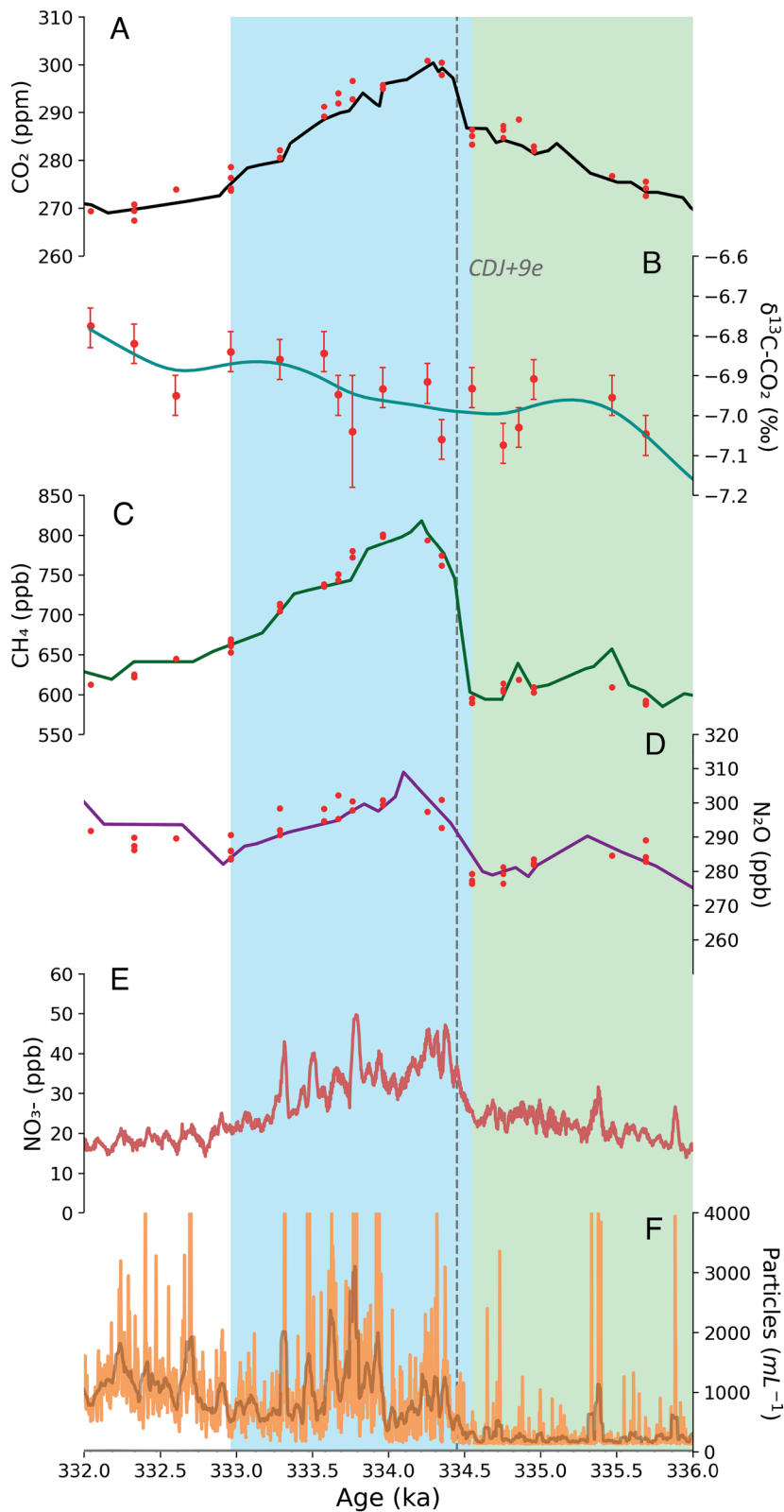


Fig. 3. CO₂ jump at the onset of MIS 9. The green box indicates the HS and blue box the overshoot. (A) EDC CO₂ concentration [black; (18)], red dots this study. (B) EDC δ¹³C-CO₂ (red dots this study, cyan corresponds to a MCA). (C) EDC CH₄ concentration (18); red dots this study. (D) EDC N₂O concentration (magenta) and red dots, this study. (E) EDC NO₃⁻ concentration [red; (41)]. (F) EDC dust particle concentration [orange and 20 point running average in dark orange; (42)]. All ice core records on the AICC23 age scale.

the end of the HS in the models due to the accumulation of heat and salt in the intermediate depth tropical Atlantic, which enters the South Labrador Sea and induces hydrostatic instabilities (56, 57).

The rapidity of the CO₂ and CH₄ increase (15 ppm and 213 ppb, respectively, within 250 y) at the onset of MIS 9 suggests that changes in atmospheric circulation accompanying the AMOC resumption are connected to these increases. The particulate dust concentration in Antarctica rises significantly and rapidly at that

point in time [Fig. 3F; (42)], while the lack of changes in snow accumulation rates at the same time (as depicted in δD) does not support any changes in dust deposition efficiency. This points at atmospheric wind patterns becoming more conducive of dust mobilization and/or transport to Antarctica in parallel to the rapid CO₂ jump, for example, by a latitudinal shift in the SO westerlies. Also, the NO₃⁻ concentration in the EDC ice core increases sharply in parallel to the concentration rise of CO₂, CH₄, and N₂O

[Fig. 3E; (41)]. Interglacial NO_3^- concentrations at EDC are controlled by postdepositional loss, and a significant increase in NO_3^- concentration through reduced postdepositional loss would require a significant increase in snow accumulation rates at that time, which is, however, not supported by the δD and deuterium excess records (40). A sudden rise of NO_3^- export from lower latitude NO_3^- sources (58) to Antarctica or a more complete local recycling of NO_x produced by photolysis of NO_3^- (59) in the snow (i.e., a reduced net loss of NO_3^- from the snowpack) due to lower wind speeds in the boundary layer on top of the snow pack could explain the NO_3^- increase observed during the CO_2 jump. In both cases, changes in local and regional atmospheric circulation in parallel to the AMOC resumption are required to explain the increase in NO_3^- . Thus, the dust and NO_3^- records provide indirect, corroborating evidence of a fast dynamical response of the SO atmosphere taking place at the same time as the CO_2 jump.

As recently outlined by Buizert et al. (22), AMOC changes not only cause the well-known millennial-scale oceanic bipolar seesaw signal but also induce a fast atmospheric teleconnection. The fast connection is likely related to a northward shift in the ITCZ in parallel to the fast NA region warming caused by an AMOC resumption. The strong impacts of an AMOC resumption and the corresponding NH warming are indicated by the change in CH_4 . Connected to the warming in the NH, the ITCZ shifted northward as indicated by local rainfall changes reconstructed, for example in stalagmites from southwest Sulawesi, Indonesia [Fig. 1R; (45)]. As a result of the abrupt precipitation increase, tropical rainforests and exposed shelf areas especially around Southeast Asia but also in the other monsoon regions are activated (45, 60) which during the MIS 9 overshoot can explain a pulse-like 213 ppb concentration increase of CH_4 .

The northward ITCZ shift is also expected to lead to a northward shift of the SH westerlies, which may then lead to enhanced upwelling of carbon-rich waters in the SO, north of the sea ice edge (25, 28), which could explain the observed jump in CO_2 in our record. Coupled carbon cycle simulations of the SH westerlies demonstrate that 10 ppm CO_2 increase or more can be explained by a northward shift of the SH westerlies (16). Boron isotope studies from deep-sea corals located in the SO demonstrate the central role of the SO as an important driver of rapid CO_2 release on centennial scales during the glacial–interglacial transition of T-I (49). Broadly speaking, the resumption of the NADW warmed the NH and led to a rapid northward shift in the westerly winds, whereas the SO cooling and sea ice increase was slower (Fig. 2). This may have created a transient condition in which sea ice was unable to shield the ocean from enhanced isopycnal mixing and outgassing, leading to a centennial-scale increase in CO_2 (49). An enhanced release of CO_2 from the Antarctic zone at the onset of MIS 9 would also be supported by southern high-latitude marine sediment records, which suggest a deepening of the lysocline, leading to increased burial rates of CaCO_3 at around 335 ka [Fig. 1P; (44)].

A decrease in land carbon storage through ecosystem changes triggered by the rapid climate change associated with the AMOC resumption could also contribute to the CO_2 jump. Based on CH_4 source estimates using CH_4 isotopes in ice cores, Riddell-Young et al. (29) estimated a coemission of pyrogenic CO_2 in parallel to rapid increases in wildfire CH_4 emissions of 5 to 10 Tg y^{-1} at the start of DO8 and DO12, which cause a CO_2 increase of comparable size as at the onset of MIS 9. At the same time, the warming and large-scale wetting of land ecosystems in the monsoon regions may also enhance carbon sequestration by land photosynthesis, which may have partly compensated the joint CO_2 release in the Southern Ocean and by wildfires.

Any of the potential CO_2 sources explaining the CO_2 jump (land carbon release, changes in air–sea–gas exchange, reduced iron fertilization, upwelling of respired carbon) require a significant negative $\delta^{13}\text{C}\text{--CO}_2$ response (48). The only exception is carbonate compensation, which, however, is too slow to be relevant for the CDJ+. Thus, the intriguing observation that the sudden enhancement of the CO_2 concentration was not accompanied by a change in the $\delta^{13}\text{C}\text{--CO}_2$ signature requires a mechanism that can compensate such a co-occurring variation in $\delta^{13}\text{C}\text{--CO}_2$. In general, a net temperature increase in global SST of 1 °C would lead to an enrichment in atmospheric $\delta^{13}\text{C}\text{--CO}_2$ of approx. 0.12‰ (61), which could have compensated for the $\delta^{13}\text{C}\text{--CO}_2$ depletion expected from upwelling or land carbon release. Unfortunately, no global SST record exists that resolves such a rapid increase in SST in parallel to the CO_2 jump. However, earth-system-model experiments show a global surface warming of a few °C within 100 to 200 y as an expected consequence of AMOC resumption (11). Based on these considerations, we suggest that the atmospheric teleconnection triggered by an AMOC resumption led to enhanced outgassing of CO_2 from the SO and/or pyrogenic net release of CO_2 from the terrestrial biosphere. At the same time, an increase in global SST, also triggered by the AMOC resumption, counteracted the anticipated decrease in the $\delta^{13}\text{C}\text{--CO}_2$.

To illustrate our interpretation and quantify a plausible history of the carbon fluxes during the overshoot at the onset of MIS 9, we used a 14-box carbon cycle model (48) as a heuristic tool to account for carbon cycle effects and to decipher potential carbon cycle processes governing the CO_2 evolution (Fig. 4). In brief, the top line of figure 4 shows three single deconvolution experiments without AMOC change where only one of the single mechanisms SST (red), SO overturning with gas-exchange (purple), and land carbon (green) was changed. We observed that none of the single mechanisms can explain the CO_2 jump—in part because they do not match the excursion in $\delta^{13}\text{C}\text{--CO}_2$. The second line of figure 4 displays double deconvolution experiments and addresses the question, whether some combinations of the single deconvolution processes can explain the changes in CO_2 and $\delta^{13}\text{C}\text{--CO}_2$. A baseline scenario is shown where the AMOC is restarted (yellow). Using this baseline, the box model explains both the CO_2 and $\delta^{13}\text{C}\text{--CO}_2$ data using either a combination of SO overturning with gas-exchange and changes in SST (Scenario 1) or changes in land carbon and SST (Scenario 2; see *SI Appendix*).

During the second phase of the overshoot (slow decline over more than 1,000 y), CO_2 , CH_4 , and N_2O concentrations show a concurrent gradual decline, whereas $\delta^{13}\text{C}\text{--CO}_2$ shows an increase. At the same time, we find a cooling in the SO region, as indicated by the EDC δD record [Fig. 1A; (36)] but consistently warm conditions in the NA as shown by the absence of *N. pachyderma* in sediment cores of ODP site 983 in the NA [Fig. 1J; (37)]. This climate evolution in both hemispheres is as expected from the bipolar seesaw coupling during a shift from reduced to intensified AMOC. During the HS preceding the CO_2 jump, the SO region slowly warms, and CO_2 is slowly released by increased upwelling in the SO, while the NA is still cold. This is also indicated by noble gas measurements in ice core samples, which show that the ocean accumulated heat during the AMOC shutdown (62). Heat release after the resumption of the AMOC leads to a global mean ocean temperature (GMOT) cooling in the millennia after the overshoot (62) while the CO_2 release from the SO is declining. Note that the slow decrease of GMOT of 2 °C after the jump also implies a solubility uptake of CO_2 equivalent to about 20 ppm [from 303 to 280 ppm; (63)]. With the NH ice sheets retreating and the

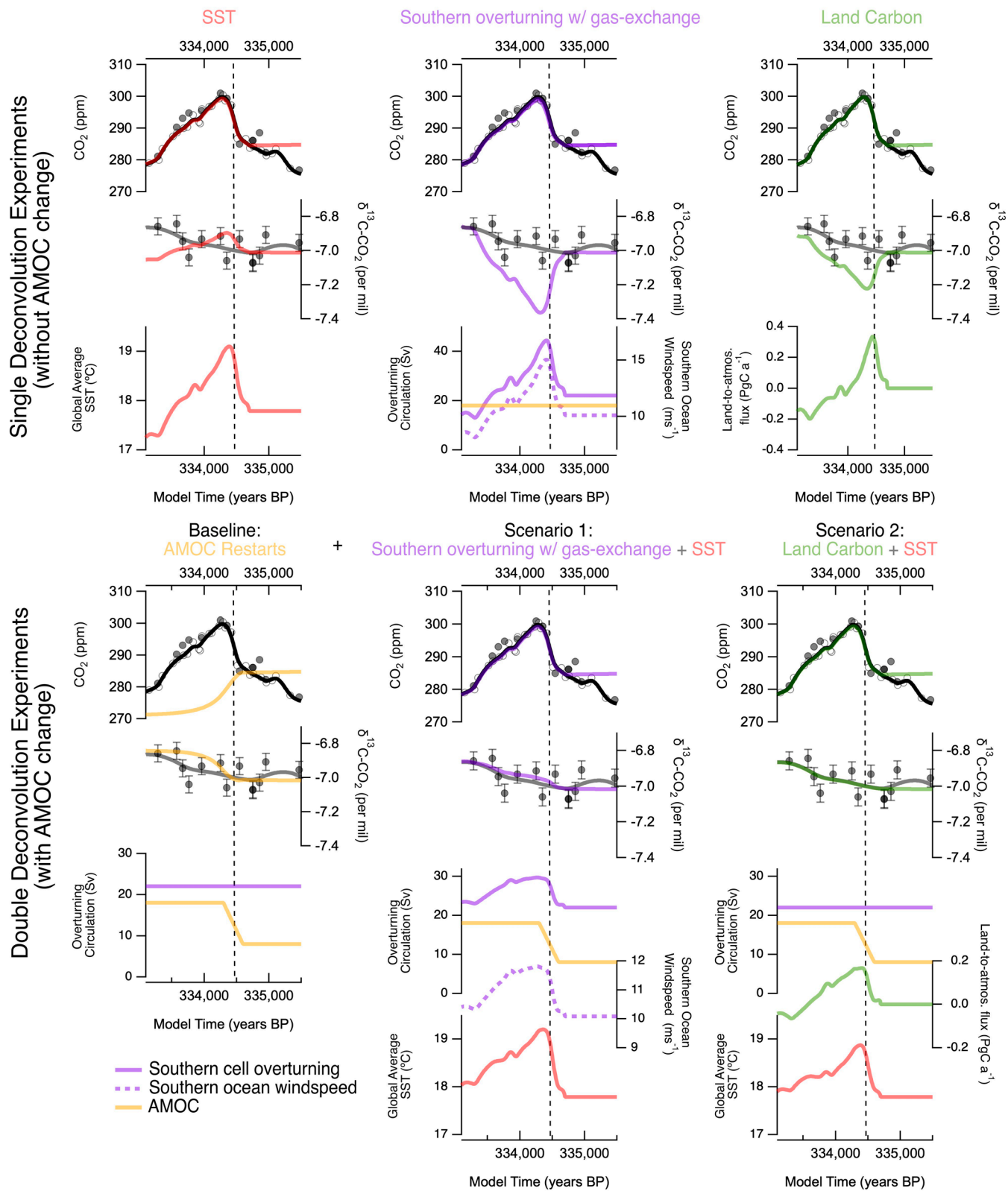


Fig. 4. Single and double deconvolution experiments conducted with a 14-box model (48) for the jump at the onset of MIS 9. *Top* panels: single deconvolution experiments showing the predicted change in $\delta^{13}\text{C-CO}_2$ if the CO₂ overshoot were due solely to changes in SST with most of the warming occurring in the North Atlantic and North Pacific (red), Southern Ocean cell overturning with gas-exchange (purple), and land carbon (green). Also shown are the summaries of the variables modified in each deconvolution experiment: global average SST (red); overturning circulation and windspeed over the SO (purple); and the land-to-atmosphere flux (green). *Bottom* panel: double deconvolution experiment showing the combined solution for CO₂ and $\delta^{13}\text{C-CO}_2$ when Southern Ocean overturning with gas-exchange and SST changes are combined (Scenario 1—purple) and land carbon with SST changes are combined (Scenario 2—green). Both these scenarios include a baseline scenario in which AMOC is restarted (yellow).

terrestrial biosphere expanding, this is also a time of increased land carbon storage and hence of slowly increasing $\delta^{13}\text{C}-\text{CO}_2$.

Conclusion

In this study, we used new high-resolution records of greenhouse gas concentrations and $\delta^{13}\text{C}-\text{CO}_2$ from the EDC ice core to investigate the rapid 15 ppm CO_2 increase at the onset of MIS 9 that parallels a sudden resumption of the AMOC. We conclude that the slow climate and greenhouse gas evolution before and after the CO_2 jump are in line with the oceanic teleconnection implied by the bipolar seesaw as seen repeatedly during the last glacial period, when the AMOC alternated between strong and weak phases. The CO_2 jump itself that occurs during the AMOC resumption represents an additional carbon cycle perturbation triggered by the atmospheric teleconnection connected to the AMOC resumption likely affecting both SO upwelling and land carbon release.

Data, Materials, and Software Availability. The data of this study have been deposited at the National Oceanic and Atmospheric Administration (NOAA) repository (<https://www.ncel.noaa.gov/access/paleo-search/study/41022>) (31).

ACKNOWLEDGMENTS. This work is part of ERC Advanced Grant project "deepSlice". The project has received funding from the European Research Council (ERC) under the European Union's Horizon 2020 research and

innovation programme (Grant agreement no. 667507). We gratefully acknowledge the financial support by the Swiss NSF (Grant numbers 200020_172506, 200020B_200328) and the Royal Society which supports TKB (URF/RV231004). TFS and LS acknowledge SNF Grant 2000_200492. E.C. received the financial support from the French National Research Agency under the 'Programme d'Investissements d'Avenir' through the HOTCLIM project (ANR-19-MPGA-0001). This work is a contribution to EPICA, a joint European Science Foundation/European Commission scientific program funded by the European Union and national contributions from Belgium, Denmark, France, Germany, Italy, the Netherlands, Norway, Sweden, Switzerland, and the United Kingdom. The main logistic support was provided by IPEV and PNRA at Dome C. This work is EPICA publication no. 325. The data of this study are available electronically at the National Oceanic and Atmospheric Administration (NOAA) repository: <https://www.ncel.noaa.gov/access/paleo-search/study/41022>.

Author affiliations: ^aClimate and Environmental Physics, Physics Institute, and Oeschger Centre for Climate Research, University of Bern, Bern 3012, Switzerland; ^bAustralian Antarctic Division, Kingston, TAS 7050, Australia; ^cAustralian Antarctic Program Partnership, Institute for Marine and Antarctic Studies, University of Tasmania, Hobart, TAS 7004, Australia; ^dLaboratory for Air Pollution/Environmental Technology, Empa—Swiss Federal Laboratory for Materials Science and Technology, Dübendorf 8600, Switzerland; ^eCommonwealth Scientific and Industrial Research Organisation, Environment Research Unit, Aspendale, VIC 3195, Australia; ^fInstitute of Environmental Geosciences, Université Grenoble Alpes, Centre National de la Recherche Scientifique, Institut de Recherche pour le Développement, Institut National de Recherche pour l'Agriculture, l'Alimentation et l'Environnement, Institut National Polytechnique de Grenoble, Grenoble 38000, France; and ^gBritish Antarctic Survey, Cambridge CB3 0ET, United Kingdom

1. B. Bereiter *et al.*, Revision of the EPICA Dome C CO_2 record from 800 to 600 ky before present. *Geophys. Res. Lett.* **42**, 542–549 (2015).
2. D. Lüthi *et al.*, High-resolution carbon dioxide concentration record 650,000–800,000 years before present. *Nature* **453**, 379–382 (2008).
3. J. R. Petit *et al.*, Climate and atmospheric history of the past 420,000 years from the Vostok ice core, Antarctica. *Nature* **399**, 429–436 (1999).
4. B. Bereiter *et al.*, Mode change of millennial CO_2 variability during the last glacial cycle associated with a bipolar marine carbon seesaw. *Proc. Natl. Acad. Sci.* **109**, 9755–9760 (2012).
5. T. F. Stocker, S. J. Johnsen, A minimum thermodynamic model for the bipolar seesaw. *Paleoceanography* **18**, 1087 (2003).
6. L. G. Henry *et al.*, North Atlantic ocean circulation and abrupt climate change during the last glaciation. *Science* **353**, 470–474 (2016).
7. J. F. McManus *et al.*, Collapse and rapid resumption of Atlantic meridional circulation linked to deglacial climate changes. *Nature* **428**, 834–837 (2004).
8. B. Stenni *et al.*, The deuterium excess records of EPICA Dome C and Dronning Maud Land ice cores (East Antarctica). *Quat. Sci. Rev.* **29**, 146–159 (2010).
9. D. Baggenstos *et al.*, Earth's radiative imbalance from the Last Glacial Maximum to the present. *Proc. Natl. Acad. Sci. U.S.A.* **116**, 14881–14886 (2019).
10. E. D. Galbraith, T. M. Merlis, J. B. Palter, Destabilization of glacial climate by the radiative impact of Atlantic Meridional Overturning Circulation disruptions. *Geophys. Res. Lett.* **43**, 8214–8221 (2016).
11. J. B. Pedro *et al.*, Beyond the bipolar seesaw: Toward a process understanding of interhemispheric coupling. *Quat. Sci. Rev.* **192**, 27–46 (2018).
12. J. A. Menking *et al.*, Multiple carbon cycle mechanisms associated with the glaciation of Marine Isotope Stage 4. *Nat. Commun.* **13**, 5443 (2022).
13. S. Eggelston *et al.*, Evolution of the stable carbon isotope composition of atmospheric CO_2 over the last glacial cycle: $\Delta^{13}\text{C}(\text{atm})$ over the last glacial cycle. *Paleoceanography* **31**, 434–452 (2016).
14. T. K. Bauska *et al.*, Controls on millennial-scale atmospheric CO_2 variability during the last glacial period. *Geophys. Res. Lett.* **45**, 7731–7740 (2018).
15. J. Schmitt *et al.*, Carbon isotope constraints on the deglacial CO_2 rise from ice cores. *Science* **336**, 711–714 (2012).
16. J. Gottschalk *et al.*, Mechanisms of millennial-scale atmospheric CO_2 change in numerical model simulations. *Quat. Sci. Rev.* **220**, 30–74 (2019).
17. T. K. Bauska, S. A. Marcott, E. J. Brook, Abrupt changes in the global carbon cycle during the last glacial period. *Nat. Geosci.* **14**, 91–96 (2021).
18. C. Nehrbass-Ahles *et al.*, Abrupt CO_2 release to the atmosphere under glacial and early interglacial climate conditions. *Science* **369**, 1000–1005 (2020).
19. E. Legrain *et al.*, Centennial-scale variations in the carbon cycle enhanced by high obliquity. *Nat. Geosci.* **17**, 1154–1161 (2024).
20. S. A. Marcott *et al.*, Centennial-scale changes in the global carbon cycle during the last deglaciation. *Nature* **514**, 616–619 (2014).
21. E. Monnin *et al.*, Atmospheric CO_2 concentrations over the last glacial termination. *Science* **291**, 112–114 (2001).
22. C. Buizer *et al.*, Abrupt ice-age shifts in southern westerly winds and Antarctic climate forced from the north. *Nature* **563**, 681–685 (2018).
23. A. Svensson *et al.*, Bipolar volcanic synchronization of abrupt climate change in Greenland and Antarctic ice cores during the last glacial period. *Clim. Past* **16**, 1565–1580 (2020).
24. R. H. Rhodes *et al.*, Paleoclimate. Enhanced tropical methane production in response to iceberg discharge in the North Atlantic. *Science* **348**, 1016–1019 (2015).
25. J. M. Lauderdale *et al.*, Wind-driven changes in Southern Ocean residual circulation, ocean carbon reservoirs and atmospheric CO_2 . *Clim. Dyn.* **41**, 2145–2164 (2013).
26. L. Menviel *et al.*, Southern hemisphere westerlies as a driver of the early deglacial atmospheric CO_2 rise. *Nat. Commun.* **9**, 2503 (2018).
27. T. Tschumi *et al.*, Deep ocean ventilation, carbon isotopes, marine sedimentation and the deglacial CO_2 rise. *Clim. Past* **7**, 771–800 (2011).
28. T. Tschumi, F. Joos, P. Parekh, How important are Southern Hemisphere wind changes for low glacial carbon dioxide? A model study. *Paleoceanography* **23**, PA4208 (2008).
29. B. Riddell-Young *et al.*, Abrupt changes in biomass burning during the last glacial period. *Nature* **637**, 91–96 (2025).
30. L. Mächler *et al.*, Laser-induced sublimation extraction for centimeter-resolution multi-species greenhouse gas analysis on ice cores. *Atmos. Meas. Tech.* **16**, 355–372 (2023).
31. F. K. Krauss, High-precision ice core measurements of CO_2 , $\delta^{13}\text{C}-\text{CO}_2$, CH_4 , and N_2O covering T-IV and the centennial-scale CO_2 jump at the onset of MIS 9. National Oceanic and Atmospheric Administration (NOAA) repository. <https://www.ncel.noaa.gov/access/paleo-search/study/41022>. Deposited 25 February 2025.
32. J. Schmitt, R. Schneider, H. Fischer, A sublimation technique for high-precision measurements of $\delta^{13}\text{C}$ and mixing ratios of CO_2 and N_2O from air trapped in ice cores. *Atmos. Meas. Tech.* **4**, 1445–1461 (2011).
33. R. Schneider *et al.*, A reconstruction of atmospheric carbon dioxide and its stable carbon isotopic composition from the penultimate glacial maximum to the last glacial inception. *Clim. Past* **9**, 2507–2523 (2013).
34. B. Bereiter *et al.*, High-precision laser spectrometer for multiple greenhouse gas analysis in 1 ml air from ice core samples. *Atmos. Meas. Tech.* **13**, 6391–6406 (2020).
35. J. Lynch-Stieglitz, The Atlantic meridional overturning circulation and abrupt climate change. *Annu. Rev. Mar. Sci.* **9**, 83–104 (2017).
36. J. Jouzel *et al.*, Orbital and millennial Antarctic climate variability over the past 800,000 y. *Science* **317**, 793–796 (2007).
37. S. Barker *et al.*, Icebergs not the trigger for North Atlantic cold events. *Nature* **520**, 333–336 (2015).
38. J. D. Hartman *et al.*, Sea-ice, primary productivity and ocean temperatures at the Antarctic marginal zone during Late Pleistocene. *Quat. Sci. Rev.* **266**, 107069 (2021).
39. S. R. Hemming, Heinrich events: Massive late Pleistocene detritus layers of the North Atlantic and their global climate imprint. *Rev. Geophys.* **42**, RG1005 (2004).
40. A. Landais *et al.*, Interglacial Antarctic–Southern Ocean climate decoupling due to moisture source area shifts. *Nat. Geosci.* **14**, 918–923 (2021).
41. R. Traversi *et al.*, High-resolution fast ion chromatography (FIC) measurements of chloride, nitrate and sulfate along the EPICA Dome C ice core. *Ann. Glaciol.* **35**, 291–298 (2002).
42. F. Lambert *et al.*, Centennial mineral dust variability in high-resolution ice core data from Dome C, Antarctica. *Clim. Past* **8**, 609–623 (2012).
43. D. A. Hodell *et al.*, A 1.5-million-year record of orbital and millennial climate variability in the North Atlantic. *Clim. Past* **19**, 607–636 (2023).
44. S. L. Jaccard *et al.*, Two modes of change in Southern Ocean productivity over the past million years. *Science* **339**, 1419–1423 (2013).
45. A. Kimbrough *et al.*, Multi-proxy validation of glacial–interglacial rainfall variations in southwest Sulawesi. *Commun. Earth Environ.* **4**, 1–13 (2023).
46. K. M. Grant *et al.*, Sea-level variability over five glacial cycles. *Nat. Commun.* **5**, 5076 (2014).
47. J. D. Shakun *et al.*, Regional and global forcing of glacier retreat during the last deglaciation. *Nat. Commun.* **6**, 8059 (2015).
48. T. K. Bauska *et al.*, Carbon isotopes characterize rapid changes in atmospheric carbon dioxide during the last deglaciation. *Proc. Natl. Acad. Sci. U.S.A.* **113**, 3465–3470 (2016).
49. J. W. B. Rae *et al.*, CO_2 storage and release in the deep Southern Ocean on millennial to centennial timescales. *Nature* **562**, 569–573 (2018).
50. N. J. Shackleton, M. A. Hall, E. Vincent, Phase relationships between millennial-scale events 64,000–24,000 y ago. *Paleoceanography* **15**, 565–569 (2000).
51. N. J. Shackleton *et al.*, Absolute calibration of the Greenland time scale: Implications for Antarctic time scales and for $\Delta^{14}\text{C}$. *Quat. Sci. Rev.* **23**, 1513–1522 (2004).

52. S. Barker *et al.*, Early interglacial legacy of deglacial climate instability. *Paleoceanography* **34**, 1455–1475 (2019).
53. Y. Sun *et al.*, Ice sheet decline and rising atmospheric CO₂ control AMOC sensitivity to deglacial meltwater discharge. *Glob. Planet. Change* **210**, 103755 (2022).
54. A. M. Seltzer *et al.*, Does δ¹⁸O of O₂ record meridional shifts in tropical rainfall?. *Clim. Past*. **13**, 1323–1338 (2017).
55. G. Deplazes *et al.*, Weakening and strengthening of the Indian monsoon during Heinrich events and Dansgaard-Oeschger oscillations. *Paleoceanography* **29**, 99–114 (2014).
56. X. Gong *et al.*, Dependence of abrupt Atlantic Meridional Ocean Circulation changes on climate background states. *Geophys. Res. Lett.* **40**, 3698–3704 (2013).
57. E. L. Deaney, S. Barker, T. van de Fliedert, Timing and nature of AMOC recovery across Termination 2 and magnitude of deglacial CO₂ change. *Nat. Commun.* **8**, 14595 (2017).
58. J. M. Burger *et al.*, A seasonal analysis of aerosol NO₃⁻ sources and NO_x oxidation pathways in the Southern Ocean marine boundary layer. *Atmos. Chem. Phys.* **23**, 5605–5622 (2023).
59. M. M. Frey *et al.*, Photolysis imprint in the nitrate stable isotope signal in snow and atmosphere of East Antarctica and implications for reactive nitrogen cycling. *Atmos. Chem. Phys.* **9**, 8681–8696 (2009).
60. Y. Chen *et al.*, Wetland expansion on the continental shelf of the northern South China Sea during deglacial sea level rise. *Quat. Sci. Rev.* **231**, 106202 (2020).
61. W. G. Mook, J. C. Bommerson, W. H. Staverman, Carbon isotope fractionation between dissolved bicarbonate and gaseous carbon dioxide. *Earth Planet. Sci. Lett.* **22**, 169–176 (1974).
62. M. Grimmer *et al.*, AMOC modulates ocean heat content during deglaciations. *Geophys. Res. Lett.* **52**, e2024GL114415 (2025).
63. R. G. Williams, M. Follows, *Ocean Dynamics and the Carbon Cycle: Principles and Mechanisms* (Cambridge University Press, 2011).